



Delft University of Technology

Analytically estimating the efficiency of high temperature aquifer thermal energy storage

Geerts, David; Daniilidis, Alexandros; Kramer, Gert Jan; Bloemendaal, Martin; Liu, Wen

DOI

[10.1186/s40517-025-00343-8](https://doi.org/10.1186/s40517-025-00343-8)

Publication date

2025

Document Version

Final published version

Published in

Geothermal Energy

Citation (APA)

Geerts, D., Daniilidis, A., Kramer, G. J., Bloemendaal, M., & Liu, W. (2025). Analytically estimating the efficiency of high temperature aquifer thermal energy storage. *Geothermal Energy*, 13(1), Article 17. <https://doi.org/10.1186/s40517-025-00343-8>

Important note

To cite this publication, please use the final published version (if applicable).
Please check the document version above.

Copyright

Other than for strictly personal use, it is not permitted to download, forward or distribute the text or part of it, without the consent of the author(s) and/or copyright holder(s), unless the work is under an open content license such as Creative Commons.

Takedown policy

Please contact us and provide details if you believe this document breaches copyrights.
We will remove access to the work immediately and investigate your claim.

RESEARCH

Open Access



Analytically estimating the efficiency of high temperature aquifer thermal energy storage

David Geerts^{1*}, Alexandros Daniilidis², Gert Jan Kramer¹, Martin Bloemendal^{2,3} and Wen Liu¹

Corresponding author at:
Copernicus Institute of
Sustainable Development,
Heidelberglaan 8, 3584 CS,
Utrecht, The Netherlands.

*Correspondence:
d.c.geerts@uu.nl

¹ Copernicus Institute
of Sustainable Development,
Utrecht University, Princetonlaan
8a, 3584 CB Utrecht, The
Netherlands

² Faculty of Civil Engineering
and Geosciences, Delft University
of Technology, Stevinweg 1, 2628
CN Delft, The Netherlands

³ TNO - Geological Survey
of the Netherlands, Princetonlaan
6, 3584 CB Utrecht, The
Netherlands

Abstract

High-Temperature Aquifer Thermal Energy Storage (HT-ATES) can be used to reduce greenhouse gas emissions from heating. The thermal recovery efficiency is the main parameter indicating the performance of an HT-ATES system and it is influenced by multiple aquifer properties and storage characteristics. This study presents a method for estimating recovery efficiency through numerical modeling, data analysis, and curve fitting. This method shows the relation between the recovery efficiency and various storage conditions, such as aquifer properties and storage temperature. In addition, this research explores an analytical relationship between energetic efficiency and recovery efficiency and verifies that relationship with the generated data. The proposed method can be used for the purpose of initial screening to estimate the performance of an HT-ATES system and for efficiently using HT-ATES as a component in larger energy system models. This method uses the modified Rayleigh number in combination with aquifer thickness and injected volume and has a R^2 of 85%. The analytical relation between energetic efficiency and recovery efficiency was shown to be accurate for all calculated energetic efficiency values above 60% and is less accurate with lower calculated energetic efficiency values.

Keywords: High-Temperature Aquifer Thermal Energy Storage (HT-ATES), Recovery efficiency, Energetic efficiency, Analytical approach

Introduction

Greenhouse gas emissions mitigation, largely due to fossil fuel based energy use, is a major challenge in the twenty-first century. The heating and cooling of buildings accounts for approximately 65% of the global energy use in buildings (IEA 2023), of which the majority is generated by fossil fuels (Cozzi et al. 2020).

Aquifer Thermal Energy Storage (ATES) systems reduce greenhouse gas emissions by storing excess thermal energy and using it when there is a demand (Hermans et al. 2018). This cycle can be repeated and is usually a seasonal cycle, storing heat during warm months and retrieving heat during cold months. This is graphically explained in Fig. 1.

In the Netherlands >3000 ATES systems have been installed. Most of these ATES systems store heat at a temperature of ≤ 25 °C (Bloemendal and Hartog 2018). This temperature range is considered to be Low-Temperature Aquifer Thermal Energy Storage (LT-ATES). When higher temperatures are used, it is called HT-ATES. Which

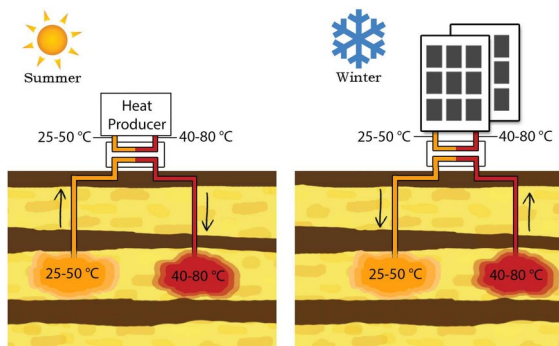


Fig. 1 Operation modes of ATES system, extracted from (Bloemendaal and Hartog 2018), left heating of the ATES system, right cooling of the ATES system, providing heat to buildings

are typically described to have a temperature range between 50 and 90 °C ((Fleuchaus et al. 2020); (Beernink et al. 2024); (Heldt et al. 2024)). ATES systems operating between a temperature of 25 and 50 °C are often called medium temperature ATES (Drijver et al. 2019). In this research HT-ATES refers to the entire range from 25 to 90 °C. Only a few HT-ATES systems are installed, most of them are experimental. Examples are described in ((Fleuchaus et al. 2020); (Opel et al. 2017); (van Loon and van der Heide 1992)).

Using HT-ATES should in theory be beneficial as higher temperatures can be used in a wider range of applications, as well as direct use for most residential heating systems. Where the application of LT-ATES in space heating systems often needs a heat pump to increase the temperature (Bloemendaal and Hartog 2018) and is most efficient in newer, well-insulated buildings. HT-ATES, however, also suffer from practical drawbacks such as increased clogging, scaling and corrosion ((Sanner and Knoblich 1999); (Holmslykke and Kjøller 2023)). Higher injected temperature can also lead to more losses and, therefore, a lower Recovery Efficiency(η_r) ((Drijver et al. 2012); (Beernink et al. 2024)). This combined with the high upfront investment costs due to the drilling of wells, makes it important to accurately predict the η_r of an HT-ATES system in a specific subsurface location.

To calculate the η_r , simulation models are used which can compute the heat losses of an HT-ATES system. These models solve the groundwater flow and heat transfer equations using numerical methods and need expertise from professionals to build and correctly run them.

Previous studies have focused on optimizing ATES systems ((Beernink et al. 2022); (Duijff et al. 2023)), yet methods for quickly estimating HT-ATES η_r remain limited. Rapid η_r estimation could facilitate the early identification of suitable sites. This paper presents a simple and computationally efficient approach to η_r estimation, offering a practical alternative to complex numerical models.

Previous research has developed similar tools to predict the η_r . An analytical approach was coined by Tang et al. (Tang and Rijnaarts 2023) that showed how the η_r can be calculated analytically. Data-driven approaches have also been proposed. Where (Schout et al. 2014) proposed a modified Rayleigh number, which was used to calculate the η_r . They specified injection temperatures between 55 °C and 90 °C and created 16 cases. Based on these cases an equation was created that used the modified Rayleigh number and which captures the relation between the model input parameters and η_r .

This temperature range was later extended to 90–300 °C by (Sheldon et al. 2021). They focused on a larger amount of cases and proposed an equation for calculating η_r based on the same modified Rayleigh number. A recent study demonstrated that the η_r can be predicted based on the ratio between the Rayleigh number and Peclet number for convection-dominated regimes. For conduction-dominated regimes, the Peclet number, in combination with the volumetric heat capacity of the aquifer, was shown to correlate with the η_r (Gao et al. 2024). All these studies showed a method for quickly determining the η_r of an ATES system.

This research extends the previous research done by Schout et al. (Schout et al. 2014) as they used a limited number of input parameter values and likely missed interactions between parameters due to this. By extending the number and range of parameter values, new insights are gained into more subtle effects not encountered in the previous study. This study also differs from the research done by Sheldon et al (Sheldon et al. 2021). The used injection temperatures in this research are lower (25–80°C instead of 90–300°C), leading to less pronounced buoyancy flow. Furthermore, compared to their study, wider ranges of parameter values for some parameters are used. Compared to Gao et al. (Gao et al. 2024) we use a larger number of parameters, where they only differed three parameters (aquifer permeability, flow rate and thermal conductivity of the cap rock), this work looks into the effects of seven different parameters. A refined version of the Rayleigh equation used by Schout et al. (Schout et al. 2014) is proposed and analyzed. This equation is simple to use and transparent in how the efficiency is calculated, offering an alternative to the numerical models.

In addition, this research introduces, explains, and analyzes the concept of Energetic Efficiency (η_e) for an HT-ATES system. The η_e quantifies the useful energy delivered by the HT-ATES to a heating system, offering a more direct and practical measure of the efficiency of HT-ATES implementation. This metric is particularly significant for evaluating HT-ATES performance within heating systems because it assesses the actual portion of extracted heat that can be effectively utilized for heating purposes. In contrast, the η_r overlooks the interaction with the heating system, making the η_e a more applicable efficiency measure within heating systems. To the authors' knowledge, this parameter has not been explicitly discussed in prior literature. Only one study (Daniilidis et al. 2022) has touched upon the η_e , exploring its impact on the techno-economic performance of an HT-ATES. In this work, we expand the knowledge by examining the relationship between η_r and η_e and presenting a formula to relate the two. To the authors' knowledge, this relationship, along with its validation, has not been previously published in the literature.

The objective of this paper is twofold. First, to develop a method for estimating the η_r , and second, to introduce, test, and analyze a relationship between η_r and η_e . Both objectives are achieved by running HT-ATES simulations using a Design of Experiments (DoE) approach over a broad yet representative range of subsurface and operational parameter values. This approach generates data on the variation in η_r and η_e . Using this data set, we evaluate the influence of each parameter on η_r and derive an equation based on the modified Rayleigh number, linking storage condition parameters to the expected η_r value. In addition, we test and validate the relationship between η_r and η_e , demonstrating its accuracy. These methods

enable the seamless integration of HT-ATES models into larger energy system models, thanks to their computational efficiency and simplicity.

Method

Definition η_r and η_e

The η_r is defined as the ratio of extracted heat to injected heat compared to the ground temperature and this factor is very important for the feasibility of an HT-ATES system. The equation for η_r is adapted from Bloemendal et al. (Bloemendal and Hartog 2018) assuming that the volume injected into the aquifer is the same as the volume extracted, which allows for unambiguous comparison of η_r values.

$$\eta_r = \frac{E_{out}}{E_{in}} = \frac{V_e \Delta T_e}{V_i \Delta T_i} = \frac{\bar{T}_e - T_g}{\bar{T}_i - T_g} \quad (1)$$

(see the nomenclature for the units used in the equations). The η_r shows the percentage of heat that is extracted compared to the injected heat. Note that in this study η_r only includes the subsurface losses, any other losses related to heat transport inside the wells or on the surface facilities are not included. The η_r changes over time, and generally increases during the first few years of operation until it stabilises. This research focuses on the stabilised η_r usually occurring after circa 8 years of operation.

An alternative approach to defining the efficiency of HT-ATES is by calculating the useful heat it delivers compared to the cutoff temperature. In district heating systems, heat is supplied to consumers at a certain temperature and returned at a lower temperature. The difference between the supply and return temperatures determines the amount of heat delivered. The return temperature, also known as the cutoff temperature, serves as the threshold, only temperatures above this threshold are considered useful for heating. Compared to the η_r , the η_e shows a direct measure of the efficiency within a heating system, where the η_r only shows the efficiency of the heating and cooling of the aquifer. The η_e is defined as:

$$\eta_e = \frac{E_{out}}{E_{in}} = \frac{V_e \Delta T_e}{V_i \Delta T_i} = \frac{V_e(\bar{T}_e - T_c)}{V_i(\bar{T}_i - T_c)} \quad (2)$$

This equation shows the percentage of useful heat extracted compared to the injected useful heat. Again this research focuses on the η_e of the eighth year, similar to the η_r . The relation between η_r and η_e is illustrated in Fig. 2. Assuming $V_e = V_i$, the η_r and η_e have the following relation:

$$\eta_e = \eta_r * \frac{T_i - T_g}{T_i - T_c} + \frac{T_g - T_c}{T_i - T_c}. \quad (3)$$

This equation is a simple analytical equation to quickly determine the η_e . However, the assumption that $V_e = V_i$ is not always correct, as extraction ceases when the extracted temperature (T_e) reaches the cutoff temperature (T_c), which also suggests that Eq. 3 may not always be correct. To examine when the equation is correct and when it is not, we compare η_e values calculated via Eq. 3, called η_f (f stands for formula) with actual η_e values from the dataset, stopping extraction at $T_e = T_c$, called η_d (d stands for data).

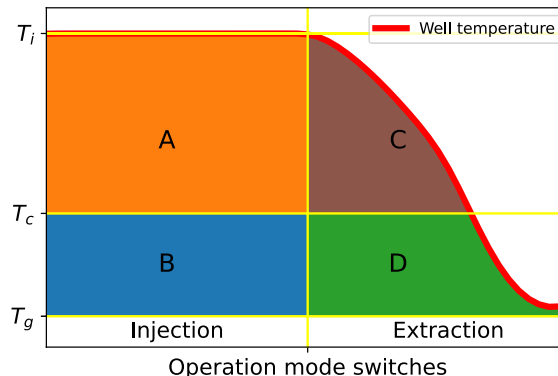


Fig. 2 Temperature of hot HT-ATES well. The $\eta_r = \frac{C+D}{A+B}$, while the $\eta_e = \frac{C}{A}$. B is not used in the η_e equation, which implies that the cold well of the system has a 100% efficiency (both η_e and η_r). This simplification is made as the primary focus of this research is focused on the hot well of the HT-ATES

Note that this calculation of η_d is an ex-post analysis after the model run as explained in "Model setup" section had been finished. η_d was calculated by using the extracted temperature profile from the model run. With this temperature profile the area C as defined in Fig. 2 is calculated and divided by the area A also defined in the same figure. Note that, in the MODFLOW model the well did not stop extracting when $T_e = T_c$; therefore, the heat in the aquifer is depleted more than when extraction stops at $T_e = T_c$. This leads to decreased η_e values, compared to when extraction would stop at $T_e = T_c$.

Two cases are considered. Both cases have a different cutoff temperature, one cutoff temperature is defined as 20°C lower than the injected temperature ($\Delta T_c = 20$) and the other as $\Delta T_c = 30$. These cases were chosen as HT-ATES is most feasible within a district heating grid and for these grids, the mentioned cutoff temperature differences are common (Naber and Dehens 2022). Where smaller ΔT_c are more common in district heating systems with low operating temperatures and larger ΔT_c are more common in district heating systems with higher operating temperatures. For both cases, the η_e calculated using Eq. 3 is compared with the η_e calculated when the extraction stops when $T_e = T_c$, which is obtained from the data.

Important parameters for η_r

The value of η_r is dependent on the amount of recoverable heat from the subsurface and, therefore, dependent on heat losses to the subsurface. Heat losses can be attributed to heat conduction and heat convection, which will displace the heat so it can not be extracted (Collignon et al. 2020). The conduction is proportional to the surface area-to-volume ratio (Doughty et al. 1982), defined as:

$$\frac{A}{V_i} = \frac{2}{r_{th}} + \frac{2}{H}, \text{ where } r_{th} = \sqrt{\frac{c_w V_i}{c_{aq} \pi H}}, \quad (4)$$

here η_r increases when V_i increases. From this equation, it can be seen that important parameters for heat loss are likely the porosity, injected volume and thickness of the aquifer. Convection is shown to be dependent on horizontal and vertical hydraulic conductivity, aquifer thickness and injected fluid temperature ((Doughty et al. 1982);

(Buscheck 1984); (van Lopik et al. 2016)). Conductive heat losses are dependent on the heat difference between the source and the surrounding, which in this case is the difference between the injected temperature and the ambient groundwater temperature. Therefore, the ambient groundwater temperature is also an important parameter.

The seven mentioned parameters and their effect on η_r are analysed in this research. A list of the parameters and the value range used for each parameter can be found in Table 4 with the respective references. This table is further explained in "Data generation" section. Anisotropy inside the aquifer is defined as

$$\alpha = k_h/k_v \quad (5)$$

Model setup

The model adopted by this research was developed in Bloemendaal et al. (Bloemendaal and Hartog 2018). The software used is MODFLOW and SEAWATv4 coupled to a transport code MT3DMS. This model uses the finite difference method to solve the groundwater flow and heat transfer equations and has been used ((Bloemendaal and Hartog 2018); (Beernink et al. 2022); (Todorov et al. 2020) and verified (Visser et al. 2015); (Mindel et al. 2021)) in previous studies. To minimize run time an axisymmetric grid was used, which was shown to be able to correctly simulate an ATES system when there is radial symmetry, which is the case here (Langevin 2008). With this approach, the results of the 2D model can be directly interpreted as equivalent to those of a 3D model, given the symmetry assumptions.

The model consists of 3 homogeneous layers, an aquifer layer of varying thickness, confined by two 30 m thick clay layers. All layers are set to have the ambient groundwater temperature at the beginning. The spatial discretization was 1 m in the vertical direction for the entire model domain. In the horizontal direction discretization was 1 m close to the well and from 200 to 2000 m away from the well, the cell size increased linearly until a cell size of 100 m is obtained at the boundary of the model, which is 2000 m away from the well. The boundaries are a constant head and constant temperature boundary, which also applies to the top and bottom edge of the model. A grid sensitivity was performed (see Sect. Appendix A) with varying grid cells size, until η_r varied less than 1% compared to smaller resolutions, this grid is visualized in Fig. 3. Any heat losses outside this aquifer domain are neglected in this study, e.g. transport losses.

One fully penetrating well is used that was located in the grid at $x = 0$. A typical HT-ATES system includes two wells; when spaced far enough apart, well interactions become negligible, allowing a single-well model to adequately capture the HT-ATES system's response. The well was assigned an injection and extraction pattern, which is a sinusoidal pattern, representing the seasonality of heat demand and supply. This pattern was 26 weeks of injecting followed by 26 weeks of extracting.

Temporal discretization of a week was used. The Courant condition is set to 0.8 in MT3DMS. MT3DMS automatically reduces time step to meet this condition, which is sufficiently small to capture important processes around the well (Bloemendaal and Hartog 2018); (Duijff et al. 2023). The simulation period was eight years, after which the operation and η_r of the HT-ATES stabilized (Beernink et al. 2024); (Sheldon et al. 2021). Other parameters used in MODFLOW can be found in Table 1.

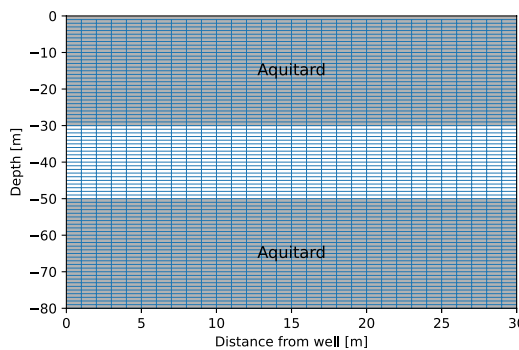


Fig. 3 Example of grid discretization used for an aquifer thickness of 20 m, where the well is located at $x = 0$. Only the first 30 ms are shown horizontally, this discretization is used until 200 ms away from the well

Table 1 Parameters used in the simulations

Parameter	Value	Unit
Density solids	2640	kg m^{-3}
Specific heat capacity solids	710	$\text{J kg}^{-1}\text{K}^{-1}$
Specific heat capacity fluids	4183	$\text{J kg}^{-1}\text{K}^{-1}$
Well radius	0.3	m
Aquitards horizontal permeability	0.05	m day^{-1}
Aquitards vertical permeability	0.01	m day^{-1}

Model verification

The created model was verified with previously published results. Multiple studies have used MODFLOW to simulate an ATES system and have proven that the simulator is accurate for such models (Visser et al. 2015); (Bonte et al. 2013); (van der Roest et al. 2021); (Bloemendaal and Hartog 2018). They also pointed out that real cases are often more complicated than the simulation and discrepancies between the software and reality exist due to this complexity.

MODFLOW/SEAWAT and MT3DMS are shown to be comparable in capabilities and results with MOOSE, MARTHE and Nexus-CSMP++ Mindel et al. 2021). The model used in this research is nonetheless compared with earlier research from (Sheldon et al. 2021 to check whether the results of the model in terms of η_r are in line with their results. While exact alignment between models is not expected due to potential differences in simulation setups (such as solver conditions or grid discretization), significant discrepancies would suggest potential modeling errors. This verification step helps identify any inconsistencies.

Eight scenarios were created to facilitate the comparison. These scenarios are based on the values of V_i , H , k_h and a as was done in (Sheldon et al. 2021). The values used in the scenarios can be found in Table 2. The scenarios exclude changes in T_i , because the lowest value used in (Sheldon et al. 2021) was already higher than the highest value in this research, and therefore, this lowest value was chosen, which was 90°C. Values for T_g and n were set in line with Sheldon et al. (Sheldon et al. 2021) and shown in Table 3.

Table 2 Scenarios for comparing the models

Name	V_i	H	k_h	a
Base	1E5	60	1	10
V^l	5E4	60	1	10
V^h	2E5	60	1	10
k^h	1E5	60	10	10
H^l	1E5	20	1	10
a^h	1E5	60	1	100
$V^l k^h H^l$	5E4	20	10	10
$V^h k^h a^h H^l$	2E5	20	10	100

The name refers to the parameters that are changed compared to the base case. The superscript refers to the direction of the change: heightened (h) or lowered (l)

Table 3 Parameters used in model verification that are different between "Model setup", "Data generation" and "Model verification" sections

Parameter	Value	Unit
Porosity	0.25	–
Ground temperature	28	°C

Table 4 Parameter ranges for simulations using a full factorial DoE. A total of 3418 forward simulations were run, of which 1458 with the DoE design and 1960 with the random design

Parameter	Used values	Unit	Source
Porosity	0.1, 0.2, 0.3	–	(Cherry and Freeze 1979)
Injected volume	$10^4, 10^5, 10^6$	m^3	(Bloemendaal and Hartog 2018)
Injected temperature	25, 52.5, 80	°C	(Bloemendaal and Hartog 2018); (Birdsell et al. 2021) ^a
Ambient ground temperature	10, 30	°C	(Bloemendaal and Hartog 2018); (Rijksoverheid 2023) ^b
Horizontal hydraulic conductivity	1, 43, 85	m day^{-1}	(Sheldon et al. 2021); (Cherry and Freeze 1979)
Anisotropy (see Eq. 5)	1, 50, 100	–	(Cherry and Freeze 1979)
Aquifer thickness	20, 62, 105	m	(Bloemendaal and Hartog 2018)

^a Definition temperature range of LT and HT-ATES

^b Common temperature at depths <500 m (depth that is outside of dutch mining regulation)

Data generation

The data were generated running simulations as described in "Model setup" section and consisted of two parts. The first part is a full factorial design, according to the DoE theory (Antony 2023). This design has the advantage that the complete parameter space is explored and every possible combination of values listed in Table 4 was modeled and the corresponding η_r was calculated. The DoE design was supplemented by using the mean values of all input parameters. These mean values were also combined with all possible other values. Two exceptions that did not use the mean were (1) ground temperature, which is expected to only influence η_r based on the difference with injected temperature (see "Important parameters for η_r " section). (2) For injected volume, the logarithmic mean was used due to the fact that

the diameter of the thermal plume of the warm well increases logarithmically and losses are shown to be dependent on the size of the thermal plume (Bloemendaal and Hartog 2018).

The second part of the data generation was based on a completely randomized design, where each parameter was randomized between its minimum and maximum value. This was done to better capture any non-linearity in the relationship between the inputs and the η_r values. 1458 forward simulations were run using the DoE design and 1960 forward simulations were run using the randomized design.

As the focus of this research is the η_r value of the hot well, the data points corresponding to a smaller injection temperature than the ambient ground temperature were removed. One example is the combination of an injected temperature of 25 °C and an ambient ground temperature of 30 °C (shown in Table 4).

η_r determination

First, a Distant-based Global Sensitivity Analysis (DGSA) (Fenwick et al. 2014) was performed to determine whether the variation in each individual parameter significantly affects the η_r value. For this analysis, the data was divided into three clusters: one containing high η_r values, one with average η_r values, and one with low η_r values. This clustering was achieved by solving the k-medoids problem (Fenwick et al. 2014). The parameter values associated with the three clusters were then compared to parameter values obtained through random sampling of the dataset, with the sampled clusters matching the size of the original three clusters. A parameter was considered significant if the difference in parameter values between the two clusters of the same size exceeded 1. Essentially showing whether changing a certain parameter, significantly changes the η_r . This DGSA analysis was used to identify parameters that do not significantly contribute to the variability in η_r , allowing them to be excluded from further analysis. This analysis was carried out using the pyDGSA package, using 3 clusters and 3000 boots (Perzan et al. 2021).

Second, the η_r value was estimated by creating an equation which equates the relevant parameters with the η_r value. This equation is simple to use compared to other methods that estimate a single number, such as machine learning. The modified Rayleigh number (Ra^*) was used as proposed by (Schout et al. 2014), who used the following formula:

$$\eta_r = Ae^{B\text{Ra}^*}. \quad (6)$$

Where A and B were originally functions of aquifer thickness and Ra^* is obtained from (Schout et al. 2014) and is

$$\text{Ra}^* = \frac{\alpha_f \bar{\rho} g H^2 c_a \sqrt{k_h k_v \Delta T}}{\bar{\mu} \lambda_a R_{th}}. \quad (7)$$

Both $\bar{\rho}$ and $\bar{\mu}$ are evaluated at the average water temperature defined as $(T_i + T_g)/2$. This research extends the curve fitting done in (Schout et al. 2014) by using a wider range of operating and subsurface conditions. A new curve is fitted using the Levenberg–Marquardt algorithm (Ranganathan 2004), as implemented in the `scipy.optimize` library (Virtanen et al. 2020).

Results

Model verification and comparison of results between one and two-wells model

The results of the eight scenarios are shown in Fig. 4. As can be seen 7 of the 8 scenarios differ by a maximum of 1%. Only one scenario differs by 2%. The observed differences can be caused by simulator setup differences and grid discretization, for example, Sheldon et al. (Sheldon et al. 2021) used a triangular grid structure that could not be replicated. Nonetheless, both simulators exhibit consistent trends in η_r with changing parameters, indicating similar parameter interactions and confirming comparable outcomes across both simulators. When the models would be set up exactly the same, the results would align even better (Mindel et al. 2021); however, this was not the objective of this verification.

Factorial design results

Table 5 presents the data created with the full factorial design. The table shows the η_r value for each of the used parameter values. This table can be used to look up η_r when the values of the parameters are close to the used values in the simulations. η_r values range from 1% to 92%, with 70% of data points being larger than 50% and 33% being larger than 80%. A general trend is that the η_r value is higher with higher injected volume, which is in line with previous research (Beernink et al. 2019). Another observation is that low anisotropy coupled with high k_h values leads to a low η_r , due to increased buoyancy flow. This effect is most prominent with high aquifer thickness due to the increased space for buoyancy flow to manifest. The highest η_r values are observed at large thickness with large injected volume and low horizontal hydraulic conductivity (having η_r values between 88%-92%).

Compared to the randomized data points, the η_r values of the DoE design are more extreme. For example the smallest η_r achieved with the randomized data points is 20%, compared to 1% of the DoE data points. The randomized data points also have a higher average η_r , which was 82% compared to 68% for the DoE data points.

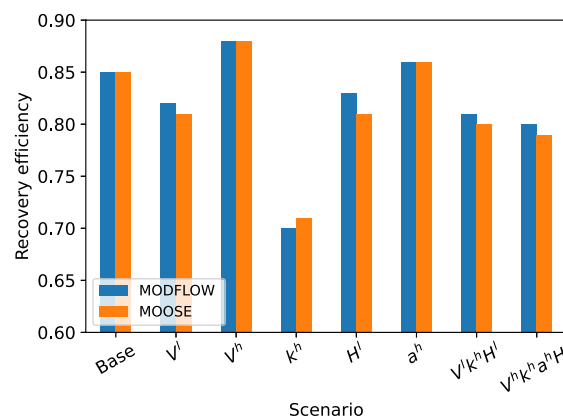


Fig. 4 Comparison with Sheldon et al. (Sheldon et al. 2021). η_r values were rounded to two significant numbers

Table 5 η_r (in %) at year eight of the simulation for each design of experiment data point

V_i	n	T_i	T_g	H	20			62			105							
				k_h	1	43	85	1	43	85	1	43	85	1	43	85		
				a	1	50	100	1	50	100	1	50	100	1	50	100		
0.1	1e4	25	10	63	63	63	56	63	63	48	62	63	62	62	48	62	62	
		10	63	63	63	29	58	61	23	49	57	61	62	62	14	60	62	
		52	30	63	63	63	36	61	62	27	58	61	62	62	20	62	62	
		80	10	60	63	63	19	40	51	14	27	38	55	62	62	7	50	57
		30	62	63	63	41	49	57	16	35	47	59	63	63	8	56	60	
	0.2	25	10	70	70	70	62	69	69	53	69	69	65	65	51	65	65	
		10	69	70	70	32	64	67	24	54	63	64	65	65	15	63	65	
		52	30	70	70	70	40	68	69	30	63	67	65	65	22	64	65	
		80	10	67	68	70	21	44	55	15	30	42	58	65	8	53	60	
		30	68	70	70	23	53	62	17	39	52	62	66	66	9	59	63	
0.3	1e5	25	10	73	73	73	65	73	73	55	73	73	67	67	53	67	67	
		10	73	73	73	33	67	71	25	57	66	66	67	67	16	65	67	
		52	30	73	73	73	41	71	72	31	66	71	67	67	24	67	67	
		80	10	70	73	73	21	46	58	16	31	44	60	67	67	8	55	56
		30	72	73	73	24	56	65	18	41	54	63	67	67	9	61	65	
	0.2	25	10	77	77	77	76	75	77	74	76	76	83	83	70	85	83	
		10	77	77	77	63	73	75	54	66	71	82	83	83	30	78	81	
		52	30	77	77	77	69	75	76	62	72	75	81	83	40	82	83	
		80	10	77	77	77	53	65	70	42	53	61	80	83	20	70	78	
		30	77	77	77	53	65	70	42	53	61	80	83	20	70	78		
0.3	1e6	25	10	82	82	82	81	82	82	79	82	82	85	85	72	85	85	
		10	82	82	82	68	78	80	58	70	75	84	85	85	31	80	83	
		52	30	82	82	82	74	80	81	68	77	80	85	85	41	84	85	
		80	10	82	82	83	51	62	69	41	48	56	79	85	18	63	74	
		30	82	83	83	56	69	75	45	57	65	82	85	85	21	73	80	
	0.2	25	10	85	85	85	83	88	86	81	84	84	92	86	86	73	86	
		10	85	85	85	69	80	82	59	72	78	85	86	86	31	82	84	
		52	30	85	85	85	76	83	84	67	79	82	86	86	42	85	84	
		80	10	84	85	85	52	64	71	42	50	58	80	86	18	65	76	
		30	85	85	85	58	71	77	46	59	67	83	86	86	21	74	81	
0.1	1e4	25	10	82	82	82	81	81	81	81	81	89	90	90	87	90	90	
		10	82	82	82	79	80	81	77	79	79	89	90	90	69	85	88	
		52	30	82	82	82	80	81	79	80	80	89	90	90	76	88	89	
		80	10	83	83	83	74	77	78	69	71	73	89	90	51	70	79	
		30	83	83	83	77	79	79	72	75	76	89	90	90	55	78	84	
	0.2	25	10	87	87	86	86	85	86	86	91	91	91	91	88	91	92	
		10	87	87	87	84	88	85	82	83	84	91	91	91	70	87	90	
		52	30	87	87	87	85	86	86	84	85	85	91	91	66	87	90	
		80	10	87	87	87	79	81	82	73	75	77	90	91	51	72	81	
		30	87	87	87	81	83	84	77	79	80	91	91	91	56	80	86	
0.3	1e5	25	10	89	89	88	88	88	88	88	92	92	92	92	85	90	92	
		10	89	89	89	86	87	88	84	85	86	92	92	92	56	82	87	
		52	30	89	89	88	87	88	88	84	87	88	92	92	37	88	90	
		80	10	89	89	89	81	83	84	75	77	80	91	92	51	74	82	
		30	89	89	89	83	85	86	79	81	83	91	92	92	43	70	80	
	0.2	25	10	89	89	88	88	88	88	92	92	92	92	92	85	90	92	
		10	89	89	89	86	87	88	84	85	86	92	92	92	51	89	91	
		52	30	89	89	89	87	88	88	84	87	88	92	92	63	91	92	
		80	10	89	89	89	81	83	84	75	77	80	91	92	27	90	85	
		30	89	89	89	83	85	86	79	81	83	91	92	92	35	84	88	

The green color refers to higher η_r values, where the red color refers to lower η_r values

Distant-based global sensitivity analysis

The DGSA shows that all of the sensitivity indices are significantly larger than one, which supports the statement that all of these parameters do influence the variance in η_r (Fig. 5). None of the parameters can be excluded based on the DGSA. What can also be seen is that four parameters should be able to explain large part of the variance in η_r , namely injected volume, injected temperature, anisotropy and horizontal hydraulic conductivity. In contrast the three remaining parameters might not be able to explain a lot of variance, which are ground temperature, porosity and aquifer thickness.

Curve fitting

A formula was fitted to the data (see Eq. 6). In Schout et al. (Schout et al. 2014) the A and B terms were functions of aquifer thickness. To check the validity of only using

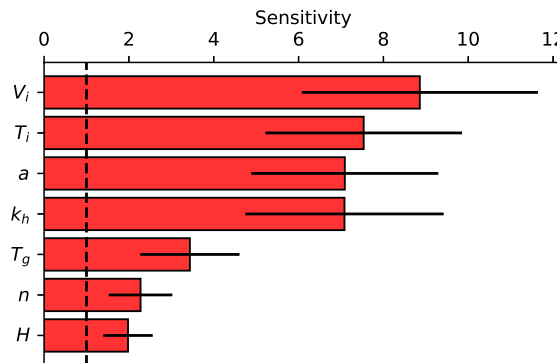


Fig. 5 Results of the DGSA with their uncertainty. A value below 1 means that the parameters does not significantly impact the η_r

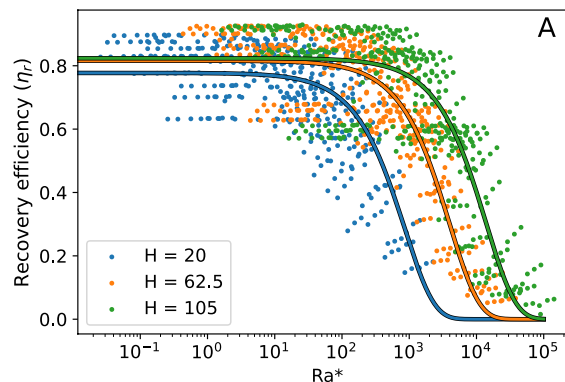
aquifer thickness, the A and B terms were tested as a function of every individual parameter. Of all parameters, only the aquifer thickness and injected volume significantly increased the R^2 compared to when A and B are single numbers and not functions of any parameter. In the case of A and B being individual numbers, the R^2 is 0.55 and A and B term values are 0.77 and $-1.0e-4$ respectively. The resulting fitting for thickness and volume can be found in Fig. 6a and b respectively. Both individual parameters have a relatively low R^2 compared to Schout et al. (Schout et al. 2014) who found an average R^2 of 94%. Therefore, injected volume and aquifer thickness are combined in one formula, which increases R^2 to 0.85 and coefficients are as follows:

$$\eta_r = (0.406 - \frac{2.02e3}{V})e^{\text{Ra}^*(\frac{2.46}{V} - 2.62e-4)} + (0.500 - \frac{1.37}{V})e^{\text{Ra}^*(\frac{-3.92e-2}{V} - 3.25e-4)} \quad (8)$$

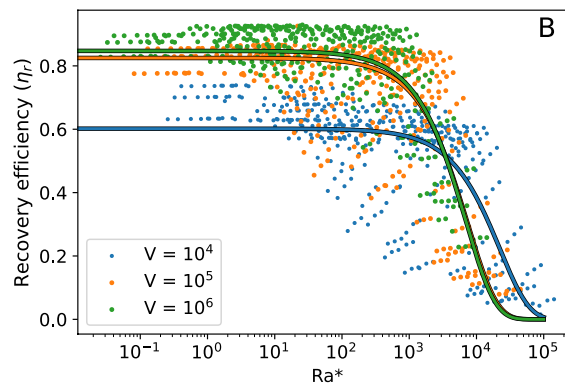
The fitting of this formula is shown in Fig. 6c. As observed, including both the injected volume and aquifer thickness enhances the formula's accuracy. This result appears to contrast with the findings of the DGSA, where aquifer thickness has the lowest sensitivity index. However, it is important to note that the DGSA provides a general analysis and using the modified Rayleigh number is a specific approach to predicting η_r . When using the modified Rayleigh number, a significant portion of the correlation between input parameters and η_r is already accounted for. The only effects not fully captured by the modified Rayleigh number are those of the injected volume and aquifer thickness.

The R^2 in this study is 9 percentage points lower than that found by Schout et al. (Schout et al. 2014) (from on average 94–85%), which can be attributed to the broader parameter range and larger dataset used here. This expanded range captures more complex interactions between parameters, indicating that the formula is accurate only within the narrower parameter limits they selected.

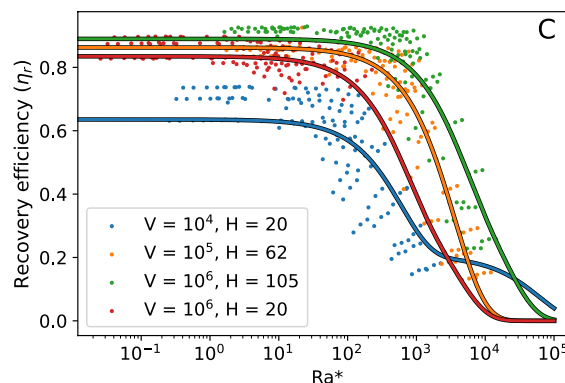
Compared to Sheldon et al. (Sheldon et al. 2021) the R^2 in this study is lower by 3 percentage point (from 88 to 85%). However, they only use aquifer thickness in their formula. This difference is due to the chosen range in aquifer thickness. The smaller aquifer thicknesses used in their work, were shown to be completely explained by the



(a) A fitted curve with Ra^* and aquifer thickness included, where $A = 0.836 + \frac{-1.16}{H}$ and $B = \frac{-2.71e-2}{H} + 1.86e-4$. R^2 of the fitted formula is 0.73.



(b) A fitted curve with Ra^* and yearly injected volume included, where $A = 0.85 + \frac{-2.48e3}{V}$ and $B = \frac{1.01}{V} - 1.46e-4$. R^2 of the fitted formula is 0.65.

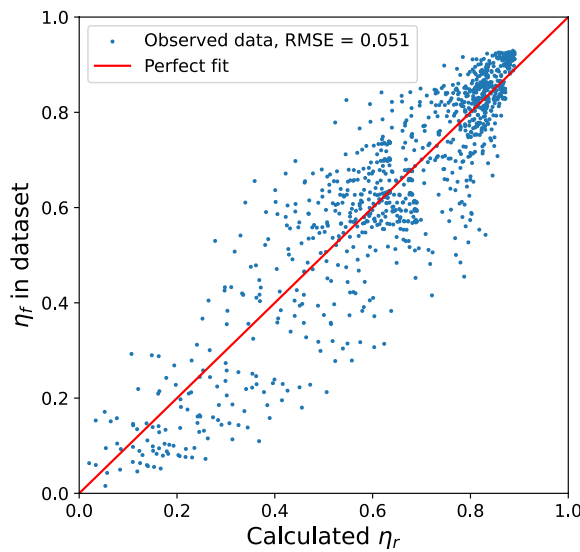


(c) A fitted curve with Ra^* , yearly injected volume and aquifer thickness included, see Eq. 8. R^2 of the fitted formula is 0.85. Only a selection of volume and thickness combinations is shown for readability.

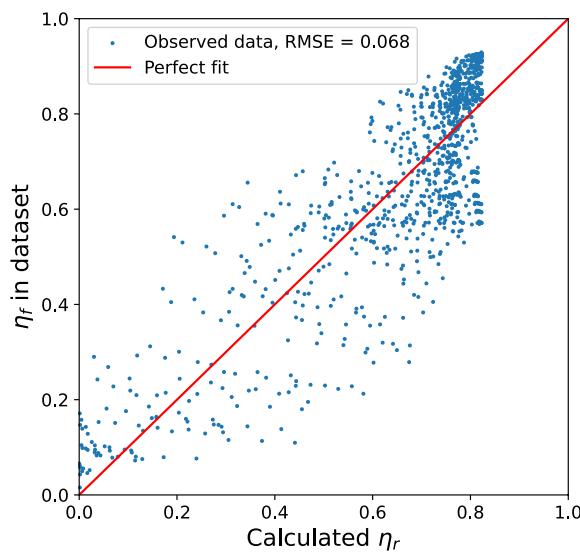
Fig. 6 Results of curve fitting

Ra^* coupled to the thickness leading to a very high R^2 . These aquifer thicknesses were not included in this research leading to a lower R^2 and the need to also include injected volume in the fitted formula. Furthermore a wider range of injected volume was used in this study. Which might increase the effect that injected volume has on η_r .

The predictive capacity of the formula was also tested using the Root Mean Square Error (RMSE) (Hodson 2022). With Eq. 8, the RMSE is reduced by 1.7 percentage points compared to only using the thickness in the fitting formula (Fig. 7). When thickness alone is used, the formula imposes a limit on η_r at 0.836 (Fig. 7b), while many data points exceed this value, reducing accuracy for higher η_r values. However, Eq. 8 resolves this problem, improving accuracy at higher η_r values. This shows that incorporating



(a) Error in the prediction using Eq. 8.



(b) Error in the prediction using A and B described in Fig. 6a.

Fig. 7 Error in the different curve fitting

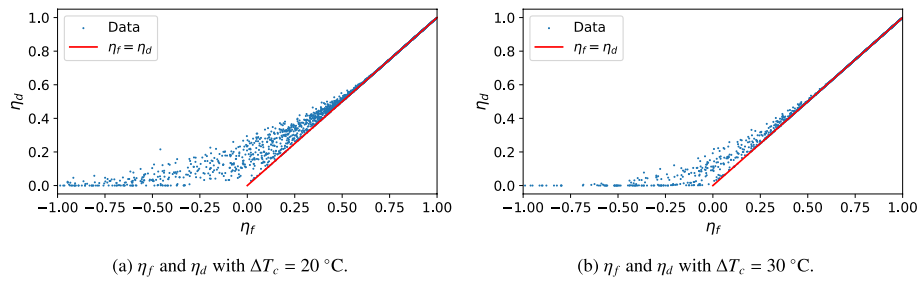


Fig. 8 η_f and η_d values for the data points considering different cutoff temperatures. Negative values occur of η_f occur when \bar{T}_e is smaller than T_c in Eq. 2

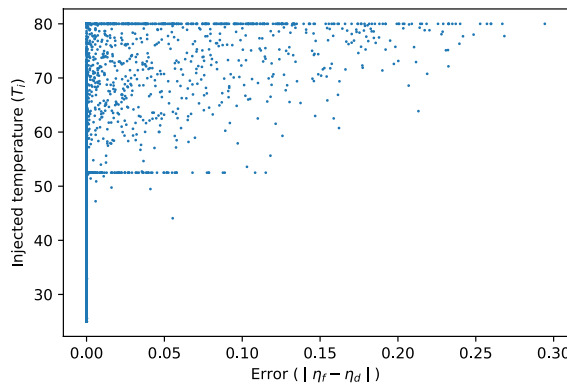


Fig. 9 Error of the formula plotted against the injected temperature with $\Delta T_c = 20$, the increased number of data points at $T_i = 80$ & 52 are due to the DoE design using only these values

injected volume into the formula enhances for both R^2 and RMSE and is important for calculating the η_r .

Difference η_r and η_e

Equation 3 can be used to calculate η_e from η_r . This part of the results explores when the equation is accurate and when it is not.

As shown in Fig. 8a, with $\Delta T_c = 20$ °C (Reminder, $\Delta T_c = T_i - T_c$), Eq. 3 is more accurate for higher η_f values. Specifically, when $\eta_f \geq 0.6$, the estimation error is less than 1% and the error tends to increase as η_f decreases. Where error is defined as $|\eta_f - \eta_d|$ and all values of η_f below zero are set to zero. This increasing error is because with a lower estimated η_f the chance that the extracted temperature reaches the cutoff temperature is larger. When that happens the assumption that $V_e = V_i$ is not valid and η_f starts to differ from η_d . This is more often the case at low η_f values, but not always and some points with low η_f have an error below 1 percentage point.

The injected temperature correlates most strongly with the error in η_f , while the other input parameters correlate only weakly with the error in η_f (Fig. 9). With larger injected temperature the errors increase on average, but even at an injected temperature of 80 °C 33% of data points have an error below 1 percentage point and 62% have an error below 5%. However, as mentioned, district heating systems operating at higher temperatures typically operate at a larger ΔT_c (Naber and Dehens 2022). The cutoff temperature significantly influences the accuracy of Eq. 3 (Fig. 8).

When the cutoff temperature decreases, ΔT_c increases, increasing the likelihood that $V_i = V_e$ since the probability of $T_c \geq T_e$ increases with a larger ΔT_c .

When the ΔT_c is 30 the differences between η_f and η_d becomes smaller and Eq. 3 is more accurate (Fig. 8b). The error is smaller than 1% for all η_f values above 0.5. HT-ATES systems with a η_e below 50% are likely less economically attractive.

Discussion

This research shows a method for quickly determining the η_r of an HT-ATES system. Furthermore it shows an analytical relation between the η_r and η_e and tests the accuracy of the relationship. This allows for quick identification of suitable locations for HT-ATES by first determining the η_r using Eq. 8 and then converting this η_r to the η_e , which shows the potential contribution of HT-ATES to a heating system. This method also facilitates integration of HT-ATES systems into larger energy system simulations without the computational burden of a detailed physics-based model.

This research also identified and tested an analytical relationship between η_r and η_e (Eq. 3) and found that this relationship is most accurate for high calculated η_e values. However, several factors may affect this accuracy. First, the model assumes 100% efficiency for the cold well, which is unrealistic; in practice, the cold well's η_r would likely resemble that of the hot well, leading to a lower calculated η_e . Second, the model assumes a fixed cutoff temperature, though in reality, this threshold can vary with external conditions. In addition, cutoff temperatures are dependent on insulation among other factors. These factors are subject to change, increasing or decreasing the cutoff temperature, and therefore, the η_e of the HT-ATES. Lastly, the η_e is calculated for data points that keep a volume balance at all times. In practice, when $T_e = T_c$, extraction would stop, leaving more heat in the subsurface, possibly increasing the η_e in subsequent years. Preliminary test suggest that this effect is minor (<2%), but future research can explore this further.

This method also has limits as the prediction of η_r can not explain all the variability in the η_r . Other methods are possible that can predict the η_r , examples are machine learning (Sheldon et al. 2021); (Geerts et al. 2025), or linear interpolation from the data in Table 5. These methods are likely to be more accurate (Zielesny 2011); however, they lack the insight that the formula in Eq. 8 offers, which showed that volume and thickness coupled to the modified Rayleigh number are the most important parameters affecting the η_r . This formulation shows analytically what parameters should change and how to increase the η_r . The proposed method was chosen due to its transparency of calculation method and simplicity, which comes at the cost of accuracy. Another approach would be to use the Peclet number, which was proposed in (Gao et al. 2024) and would be an alternative approach for future research. Another limitation is that the equation still requires detailed information on the subsurface, which has to be measured or estimated before this equation can be used.

To make a feasibility assessment for an HT-ATES installation, there are other considerations that need to be taken into account to be able to use the results of this research appropriately. These considerations can be divided into four types:

1. Other subsurface conditions not studied in this work might need investigation. First, other nearby wells or boreholes can positively or negatively affect the η_r of the HT-ATES system, e.g. nearby ATES systems or BTES systems. In Duijff et al. (Duijff et al. 2023) it was determined that the mutual interaction effect of ATES can be minimized by placing them far apart. However, this spacing is often not possible due to practical constraints such as the piping and other underground activities (Çomaklı et al. 2004). Consequently the HT-ATES wells are placed closer together and they might interact with each other, influencing the η_r . Second, is the ambient groundwater flow, that can affect the η_r . Bloemendaal et al. (Bloemendaal and Hartog 2018) showed that change in η_r related to ambient groundwater flow in the aquifer can be written in relation to r_{th}/u . They also showed that when groundwater flow is higher, the ratio $\frac{L}{r_{th}}$ should be below 1, where L is the injection screen length. Another study showed that the ambient groundwater flow can be advantageous if well design is adapted, which was coined to be a unidirectional ATES (Silvestri et al. 2025). Lastly, the aquifer was assumed to be homogeneous, despite the expectation of heterogeneity in real-world aquifers (Visser et al. 2015). Aquifer heterogeneity is highly site-specific, and its effect on the η_r depends on the type and extent of heterogeneity present. Previous studies have shown that heterogeneity influences both the η_r and the thermal distribution of the hot plume (Visser et al. 2015); (Sommer et al. 2013). The impact of heterogeneity on η_r can vary significantly; for instance, Visser et al. (Visser et al. 2015) reported a reduction in η_r due to heterogeneity in their specific case study. However, due to the site-specific nature of these effects, heterogeneity was not considered in this work.
2. System-level considerations such as the availability of heat demand and proximity to heat transport infrastructure is crucial to be able to use the stored heat efficiently and minimize transport losses, which were found to be between 5-35% and should be taken into account (Werner 2017).
3. Regulations have to be taken into account in the decision-making. Examples are that some areas or aquifers are protected due to drinking water extraction (Stemmle et al. 2022) or restrictive use of the subsurface area (Bloemendaal et al. 2018).
4. Lastly the economic feasibility of the HT-ATES system depends on factors such as price of heat used for charging and the price of the stored heat, cost of drilling, the optional installation of an heat pump and possible subsidy schemes for HT-ATES (Daniilidis et al. 2022). Previous research has shown that η_r alone is not a sufficient predictor for good economic performance (Daniilidis et al. 2022); (Beernink et al. 2022) and that a minimum transmissivity and system capacity is required to make HT-ATES competitive with other storage options (Daniilidis et al. 2022).

All these consideration are important for the successful installation and operation of an HT-ATES system.

Conclusion

In this research a method was developed to estimate the η_r value of an HT-ATES system for temperatures in the range of 25-80 °C. First, a numerical model was built to represent the subsurface part of an HT-ATES system. The model was validated with (Sheldon et al. 2021) and the models show comparable η_r values.

The model was then run repeatedly for a wide range of relevant subsurface and design parameters to generate data on the relationship between these input parameters and the η_r values. Based on this data, an equation was fitted to the data using the modified Rayleigh number. This equation achieved an R^2 of 85% and offers robust predictive capability for η_r within the tested parameter range (Eq. 8). In addition, Table 5 was presented from which the η_r can be read when the parameters are known. This table has the exact simulation outcomes. Both the equation and the table can be used to identify suitable HT-ATES sites, after which more detailed modelling might still be necessary depending on the location's unique situation.

An analytical relation between the η_e and η_r was developed and tested (Eq. 3). It was shown that the used relation is accurate for those data points where the calculated η_e is larger than 50% when the difference between injected temperature and cutoff temperature is 30°C. Using a difference of 20°C this threshold is 60%. Below these thresholds, the η_e estimate may be less precise but can still offer a useful indication for feasibility assessment. HT-ATES systems with η_e values below this threshold are likely not feasible from an economic perspective and further investigation for these cases would be needed.

With this research first the η_r can be estimated using the proposed formula (Eq. 8) after which the η_e can be calculated using Eq. 3. Coupling these two equations shows the efficiency of an HT-ATES within an heating system. By coupling the two equations, suitable HT-ATES sites can be quickly identified and the usefulness of the HT-ATES within a heating system can be calculated.

Appendix

Grid sensitivity

This section presents the grid sensitivity analysis performed to evaluate the impact of grid block size on the calculated η_r . For 10 randomly selected points in the DoE design the difference in η_r was calculated between different grid block sizes. The following grid block sizes were used:

1. 0.25 x 0.25 (x-direction x z-direction) m blocks
2. 0.5 x 0.5 m blocks
3. 1 x 0.5 m blocks
4. 0.5 x 1 m blocks
5. 1 x 1 m blocks
6. 2 x 2 m blocks

The baseline simulation was conducted using 0.25 x 0.25 m grid blocks, and all other grid sizes were compared to this baseline. The relative difference, σ , was calculated using the following equation:

$$\sigma = \eta_r - \eta_{r,base}. \quad (9)$$

where $\eta_{r,base}$ is the η_r of the simulation using grid blocks of 0.25 x 0.25 m.

Table 6 shows the resulting σ . The 1 x 1 m has both the average and maximum σ below 1%, while for the 2 x 2 m blocks both the average and maximum σ are above 1%. Therefore, the 1 x 1 blocks were used.

Abbreviations

α_f	Coefficient of thermal expansion of water K^{-1}
ΔT	Difference between injected and ground temperature $^{\circ}C$
η_e	Energetic efficiency -
η_f	Energetic efficiency calculated using the data -
η_f	Energetic efficiency calculated with Eq. 3 -
η_r	Thermal recovery efficiency -
λ_a	Thermal conductivity aquifer m^2
$\bar{\mu}$	Viscosity of water at average of T_i, T_g Pa s
$\bar{\rho}$	Density of water at average of $T_i, T_g K^{-1}$
\bar{T}_i	Average injected temperature $^{\circ}C$
\bar{T}_o	Average extracted temperature $^{\circ}C$
π	Pythagoras number -
A	Surface area of a cylinder m^2
a	Anisotropy -
c_w	Volumetric heat capacity of water $Jm^{-3}K^{-1}$
c_{aq}	Volumetric heat capacity of saturated aquifer $Jm^{-3}K^{-1}$
E_{in}	Energy injected into well J
E_{out}	Energy extracted out of well J
g	Acceleration due to gravity ms^{-2}
H	Thickness aquifer m
K_h	Horizontal permeability m^2
k_h	Horizontal hydraulic conductivity $m day^{-1}$
K_v	Vertical permeability m^2
k_v	Vertical hydraulic conductivity $m day^{-1}$
n	Porosity of aquifer -
r_h	Hydraulic thermal radius of a well m
r_{th}	Theoretical thermal radius of a well m
T_c	Cutoff temperature $^{\circ}C$
T_e	Temperature of extracted water $^{\circ}C$
T_g	Ambient groundwater temperature $^{\circ}C$
T_i	Temperature of injected water $^{\circ}C$
u	Background groundwater flow $m day^{-1}$
V_e	Extracted water volume during one extraction period, which is in this research a single year m^3
V_i	Injected water volume during one storage period, which is in this research a single year m^3

Author contributions

David Geerts: conceptualization, methodology, software, validation, investigation, data curation, writing—original draft, and visualization. Alexandros Daniilidis: methodology, software, writing—review and editing, supervision, and funding

Table 6 Average and maximum σ values obtained from the grid sensitivity analysis for the 10 data points tested

Block size	Average σ (%)	Highest σ (%)
0.5 x 0.5m	0.02	0.08
0.5 x 1m	0.07	0.20
1 x 0.5m	0.08	0.18
1 x 1m	0.15	0.35
2 x 2m	1.1	3.2

acquisition. Gert Jan Kramer: writing—review and editing and supervision. Martin Bloemendaal: methodology, software, writing—review and editing, supervision, and funding acquisition. Wen Liu: methodology, writing—review and editing, visualization, supervision, and funding acquisition.

Funding

This work was funded by the European Union under the Horizon Europe programme (grant no. 1011096566). Views and opinions expressed are, however, those of the author(s) only and do not necessarily reflect those of the European Union or CINEA. Neither the European Union nor CINEA can be held responsible for them.

Availability of data and materials

The data generated during the research is available at: https://github.com/dayfix/DD_ATES.

Declarations

Competing interests

The authors declare that they have no known competing financial interests or personal relationships that could have appeared to influence the work reported in this paper.

Received: 12 December 2024 Accepted: 1 April 2025

Published: 22 April 2025

References

Antony J. Design of experiments for engineers and scientists. Amsterdam: Elsevier; 2023.

Beernink S, Hartog N, Bloemendaal M, van der Meer M. Ates systems performance in practice: Analysis of operational data from ates systems in the province of utrecht, the netherlands. In Proceedings of the European Geothermal Congress, 2019.

Beernink S, Bloemendaal M, Kleinlugtenbelt R, Hartog N. Maximizing the use of aquifer thermal energy storage systems in urban areas: effects on individual system primary energy use and overall ghg emissions. *Appl Energy*. 2022;311:118587.

Beernink S, Hartog N, Vardon PJ, Bloemendaal M. Heat losses in ates systems: the impact of processes, storage geometry and temperature. *Geothermics*. 2024;117:102889.

Birdsell DT, Adams BM, Saar MO. Minimum transmissivity and optimal well spacing and flow rate for high-temperature aquifer thermal energy storage. *Appl Energy*. 2021;289:116658.

Bloemendaal M, Hartog N. Analysis of the impact of storage conditions on the thermal recovery efficiency of low-temperature ates systems. *Geothermics*. 2018;71:306–19.

Bloemendaal M, Jaxa-Rozen M, Olsthoorn T. Methods for planning of ates systems. *Appl Energy*. 2018;216:534–57.

Bonte M, Van Breukelen BM, Stuyfzand PJ. Environmental impacts of aquifer thermal energy storage investigated by field and laboratory experiments. *J Water Clim Change*. 2013;4(2):77–89.

Buscheck TA. The hydrothermal analysis of aquifer thermal energy storage. Berkeley: University of California; 1984.

Cherry JA, Freeze RA. Groundwater. Englewood Cliffs: Prentice-Hall; 1979.

Collignon M, Klemetsdal ØS, Møyner O, Alcanié M, Rinaldi AP, Nilsen H, Lupi M. Evaluating thermal losses and storage capacity in high-temperature aquifer thermal energy storage (ht-ates) systems with well operating limits: insights from a study-case in the greater Geneva Basin, Switzerland. *Geothermics*. 2020;85:101773.

Çomaklı K, Yüksel B, Çomaklı Ö. Evaluation of energy and exergy losses in district heating network. *Appl Therm Eng*. 2004;24(7):1009–17.

Cozzi L, Gould T, Bouckart S, Crow D, Kim T, Mcglade C, Olejarnik P, Wanner B, Wetzel D. World energy outlook 2020. IEA: Paris, France. 2020; 2050:1–461.

Daniilidis A, Mindel JE, De Oliveira Filho F, Guglielmetti L. Techno-economic assessment and operational co2 emissions of high-temperature aquifer thermal energy storage (ht-ates) using demand-driven and subsurface-constrained dimensioning. *Energy*. 2022;249:123682.

Doughty C, Hellström G, Tsang CF, Claesson J. A dimensionless parameter approach to the thermal behavior of an aquifer thermal energy storage system. *Water Resour Res*. 1982;18(3):571–87.

Drijver B, van Aarsen M, Zwart BD. High-temperature aquifer thermal energy storage (ht-ates): sustainable and multi-useable. *Proceedings of the Innostock*. 2012; 1–10.

Drijver B, Bakema G, Oerlemans P. State of the art of ht-ates in the netherlands. In European Geothermal Congress: Proceedings. Netherlands: Den Haag; 2019.

Duijff R, Bloemendaal M, Bakker M. Interaction effects between aquifer thermal energy storage systems. *Groundwater*. 2023;61(2):173–82.

Fenwick D, Scheidt C, Caers J. Quantifying asymmetric parameter interactions in sensitivity analysis: application to reservoir modeling. *Math Geosci*. 2014;46:493–511.

Fleuchaus P, Schüpler S, Bloemendaal M, Guglielmetti L, Opel O, Blum P. Risk analysis of high-temperature aquifer thermal energy storage (ht-ates). *Renew Sustain Energy Rev*. 2020;133:110153.

Gao H, Zhou D, Tatomir A, Li K, Ganzer L, Jaeger P, Brenner G, Sauter M. Estimation of recovery efficiency in high-temperature aquifer thermal energy storage considering buoyancy flow. *Water Resour Res*. 2024;60(11):e2024WR037491.

Geerts D, Daniilidis A, Liu W. A fast and accurate data-driven model for estimating the production temperature of high-temperature aquifer thermal energy storage. Under Rev. 2025.

Heldt S, Beyer C, Bauer S. Uncertainty assessment of thermal recovery and subsurface temperature changes induced by high-temperature aquifer thermal energy storage (ht-ates): a case study. *Geothermics*. 2024;122:103086.

Hermans T, Nguyen F, Klepikova M, Dassargues A, Caers J. Uncertainty quantification of medium-term heat storage from short-term geophysical experiments using Bayesian evidential learning. *Water Resour Res*. 2018;54(4):2931–48.

Hodson TO. Root mean square error (rmse) or mean absolute error (mae): When to use them or not. *Geosci Model Dev Discuss*. 2022;2022:1–10.

Holmslykke HD, Kjøller C. Reactive transport modelling of potential near-well mineralogical changes during seasonal heat storage (ht-ates) in Danish geothermal reservoirs. *J Energy Storage*. 2023;72:108653.

IEA, "Space heating," IEA, Tech Rep. 2023. <https://www.iea.org/reports/space-heating>

Langevin CD. Modeling axisymmetric flow and transport. *Groundwater*. 2008;46(4):579–90.

Mindel JE, Alt-Epping P, Les Landes AA, Beernink S, Birdsall DT, Bloemendaal M, Hamm V, Lopez S, Maragna C, Nielsen CM, et al. Benchmark study of simulators for thermo-hydraulic modelling of low enthalpy geothermal processes. *Geothermics*. 2021;96:102130.

Naber N, Dehens J. Update kentallen installaties vesta mais. CE Delft Tech Rep. 2022. https://ce.nl/wp-content/uploads/2023/03/CE_Delft_210348_Update_kentallen_installaties_Vesta_MAIS_Def.pdf. Accessed 28 Nov 2024

Opel O, Strodel N, Werner K, Geffken J, Tribel A, Ruck W. Climate-neutral and sustainable campus Leuphana University of Lueneburg. *Energy*. 2017;141:2628–39.

Perzan Z, Babey T, Caers J, Bargar J, Maher K. Local and global sensitivity analysis of a reactive transport model simulating floodplain redox cycling. *Water Resour Res*. 2021;57(12):e2021WR029723.

Ranganathan A. The levenberg-marquardt algorithm. *Tutorial LM Algorithm*. 2004;11(1):101–10.

Rijksoverheid. Mijnbouwwet. 2023. <https://wetten.overheid.nl/BWBR0014168/2023-07-01>

Sanner B, Knoblich K. Advantages and problems of high temperature underground thermal energy storage. *Bull d'Hydrogéol*. 1999;17:341–8.

Schout G, Drijver B, Gutierrez-Neri M, Schotting R. Analysis of recovery efficiency in high-temperature aquifer thermal energy storage: a Rayleigh-based method. *Hydrogeol J*. 2014;22(1):281.

Sheldon HA, Wilkins A, Green CP. Recovery efficiency in high-temperature aquifer thermal energy storage systems. *Geothermics*. 2021;96:102173.

Silvestri V, Crosta G, Previati A, Frattini P, Bloemendaal M. Uni-directional ates in high groundwater flow aquifers. *Geothermics*. 2025;125:103152.

Sommer W, Valstar J, van Gaans P, Grotenhuis T, Rijnaarts H. The impact of aquifer heterogeneity on the performance of aquifer thermal energy storage. *Water Resour Res*. 2013;49(12):8128–38.

Stemmle R, Hammer V, Blum P, Menberg K. Potential of low-temperature aquifer thermal energy storage (lt-ates) in Germany. *Geotherm Energy*. 2022;10(1):1–25.

Tang DW, Rijnaarts HH. Dimensionless thermal efficiency analysis for aquifer thermal energy storage. *Water Resour Res*. 2023;59(11):e2023WR035797.

Todorov O, Alanne K, Virtanen M, Kosonen R. Aquifer thermal energy storage (ates) for district heating and cooling: a novel modeling approach applied in a case study of a Finnish urban district. *Energies*. 2020;13(10):2478.

van Loon L, van der Heide K. High-temperature ates at the university of Utrecht, The Netherlands. SAE Techn Paper Tech Rep. 1992. <https://doi.org/10.4271/929053>.

van Lopik JH, Hartog N, Zaandordijk WJ, et al. The use of salinity contrast for density difference compensation to improve the thermal recovery efficiency in high-temperature aquifer thermal energy storage systems. *Hydrogeol J*. 2016;24(5):1255–1271.

van der Roest E, Beernink S, Hartog N, van der Hoek JP, Bloemendaal M. Towards sustainable heat supply with decentralized multi-energy systems by integration of subsurface seasonal heat storage. *Energies*. 2021;14(23):7958.

Virtanen P, Gommers R, Oliphant TE, Haberland M, Reddy T, Cournapeau D, Burovski E, Peterson P, Weckesser W, Bright J, van der Walt SJ, Brett M, Wilson J, Millman KJ, Mayorov N, Nelson ARJ, Jones E, Kern R, Larson E, Carey CJ, Polat İ, Feng Y, Moore EW, VanderPlas J, Laxalde D, Perktold J, Cimrman R, Henriksen I, Quintero EA, Harris CR, Archibald AM, Ribeiro AH, Pedregosa F, van Mulbregt P, SciPy 1.0 Contributors. SciPy 1.0: fundamental algorithms for scientific computing in python. *Nat Methods*. 2020;17:261–72.

Visser PW, Kooi H, Stuyfzand PJ. The thermal impact of aquifer thermal energy storage (ates) systems: a case study in the Netherlands, combining monitoring and modeling. *Hydrogeol J*. 2015;23(3):507.

Werner S. International review of district heating and cooling. *Energy*. 2017;137:617–31.

Zielenay A. From curve fitting to machine learning. Berlin: Springer; 2011. p. 18.

Publisher's Note

Springer Nature remains neutral with regard to jurisdictional claims in published maps and institutional affiliations.